Dynamic Article Links ▶

PAPER

Bioinspired synthesis of gadolinium-based hybrid nanoparticles as MRI blood pool contrast agents with high relaxivity†

Bingbo Zhang,‡*[a] Hantao Jin,‡[b] Yan Li,[c] Bingdi Chen,[a] Shiyuan Liu[b] and Donglu Shi*[ad]

A unique biomineralization approach was developed to synthesize gadolinium-based hybrid (GH) nanoparticles for effective blood pool contrast agents. This approach is bioinspired, environmentally benign, and straightforward. As-prepared GH nanoparticles are biocompatible and well stable in serum. They exhibit much higher longitudinal relaxivity and transverse relaxivity in water (r_1 and r_2 values of 15.0 and 19.7 s^{-1} per mM of Gd^{3+}, respectively) than those measured for Gd–DTPA solution (r_1 and r_2 values of 3.7 and 4.6 s^{-1} per mM of Gd^{3+}, respectively). *In vivo* T_1-weighted magnetic resonance imaging (MRI) in living mice shows that the GH nanoparticles have an intravascular half-life up to 1 h, much longer than that of Gd–DTPA (about 10 min). As the GH nanoparticles were found to be cleared gradually *via* hepatobiliary (HB) processing, they can also serve as ideal candidates for liver specific MR contrast agents. In particular, these GH nanoparticles are bioinspired and environmentally benign, therefore promising for medical imaging applications.

1. Introduction

Blood pool contrast agents (BPCAs) are highly desirable in contrast-enhanced magnetic resonance angiography (CE-MRA).[1,2] BPCA-based CE-MRA can be supplemented with time-resolved angiography, flow measurement, vessel wall imaging, and plaque characterization for comprehensive assessment of vascular disease. In comparison with extracellular contrast agents, BPCAs have several advantages, which include lower leakage into the interstitial space and longer intravascular half-life.[3–5] However, only gadofosveset (Vasovist®, Bayer Schering Pharma AG) has so far been approved for clinical MRA in Europe and aortoiliac MRA in USA.[6] Most of BPCAs are designed as either gadolinium containing small molecules that bind to serum albumin,[7–9] or macromolecules,[10–12] which can slow down leakage through endothelial pores and extend the imaging window from approximately one minute to one hour.

Recently, a different type of BPCA has been developed based on superparamagnetic iron oxide (SPIO)[13] or gadolinium hybrid nanoparticles.[14–16] Nanoparticles are an attractive form of BPCAs in diagnostics for their superb pharmacokinetic properties and enhanced permeability and retention (EPR) effect.[17] They can effectively prolong the circulation time and increase signal-to-noise ratio. Nonetheless, most of the nanoparticulated contrast agents (CAs) are based on iron oxides, which have high r_2/r_1 values, making them negative CAs. On the other hand, some ultra-fine SPIO or gadolinium hybrid nanoparticulate CAs have low r_2/r_1 and high r_1 values, leading to positive CAs.[14–16,18] S. Srivastava reported citrate-coated Fe_3O_4 nanoparticles (6 nm) with a narrow size distribution, synthesized by "one-pot green chemistry route" in diethylene glycol (DEG) solvent. Their low value of relaxivities ratio ($r_2/r_1 = 1.46$) indicates the T_1 contrast.[19] Gadolinium-based agents have special advantages due to its large magnetic moments (seven unpaired electrons),[20–22] particularly useful for MRI of different organs such as liver,[23] spleen,[24] and vascular[25] (iron oxide is more specific to liver[26]). Currently, various gadolinium hybrid nanoparticulates are synthesized for MRI applications due to their unique properties such as high molecular weight (prevents quick renal excretion) and high r_1 relaxivity. For example, 2.2 nm gadolinium oxides nanoparticles were synthesized by a modified "polyol" protocol at 180 °C for 4 h. They have an r_1 value of 8.8 s^{-1} per mM of Gd^{3+}.[15] Gd (BDC) $1.5(H_2O)_2$ nanorods (BDC is 1,4-benzendicarboxylate), synthesized using the reverse microemulsions have an r_1 value of 35.8 s^{-1} per mM of Gd^{3+};[18] while the $GdPO_4$ nanoparticles prepared with the well-known hydrothermal synthesis present an r_1 value of 13.9 s^{-1} per mM of

[a]*The Institute for Advanced Materials & Nano Biomedicine, Tongji University School of Medicine, Shanghai 200092, China. E-mail: bingbozhang@tongji.edu.cn; Fax: +86-21-65983706-0; Tel: +86-21-65983706-819*

[b]*Department of Radiology, ChangZheng Hospital, the Second Military Medical University, No. 415 Fengyang Road, Shanghai 200003, China*

[c]*Shanghai First Maternity and Infant Hospital, Tongji University, Shanghai 200040, China*

[d]*School of Electronic and Computing Systems, University of Cincinnati, Cincinnati, OH 45221-0012, USA. E-mail: donglu.shi@uc.edu*

† Electronic supplementary information (ESI) available. See DOI: 10.1039/c2jm30629h

‡ These authors contributed equally to this work.

Gd³⁺.[16] However, the above mentioned gadolinium-based nanoparticles are prepared at high temperatures with complicated chemical procedures. It is therefore important to develop simple approaches for the preparation of the gadolinium-based nanoparticles. For example, ultra fine (1–3 nm) gadolinium oxide (Gd_2O_3) nanoparticles have been prepared at the short synthesis time (1 h) and moderate temperature (60 °C) using citric acid as a capping agent.[27]

Most of the reported synthesis methods are energy-consuming, requiring stringent conditions (*e.g.*, pH adjusting, high temperature and pressure). Furthermore, the quantities produced are limited with low reproducibility due to complexities involved in the controlling reaction processes.[28] In contrast, nanomaterials *via* bioinspired biomineralization can be developed in a moderate and controlled fashion. The biomolecule-based materials have been well established with elaborate mineral structures at ambient temperatures. These nanomaterials produced by bioinspired biomineralization present significantly improved performances in medical diagnosis over those prepared by traditional chemical synthesis. In bioinspired biomineralization, the biomacromolecules are employed to collect and transport raw materials and assemble them into ordered composites with consistency and uniformity in an aqueous environment under mild conditions. There have been a variety of nanomaterials prepared by bioinspired biomineralization. These include gold nanocluster,[29] gold nanoparticles[30] and semiconductor nanocrystals.[31–33]

In this study, we report a unique approach by which the inorganic–organic gadolinium-based hybrid (GH) nanoparticles are synthesized *via* biomineralization. Biomineralization is achieved from a suspension of gadolinium(III) chloride hexahydrate, bovine serum albumin (BSA), and sodium hydroxide water solution in a straightforward, environmentally benign, one-pot, and reproducible synthetic route at room temperature. The synthesis is similar to biomineralization of organisms in nature: sequestering and interacting with inorganic ions, followed by providing scaffolds for the minerals formed. This method has been successfully used in the synthesis of fluorescent gold nanoclusters.[29] The BSA molecules sequester the Gd ions and entrap them upon adding Gd(III) ions into the aqueous BSA solution. The scaffold ability of BSA molecules is then activated by adjusting the pH to 12 and the entrapped ions in a progressive reaction to form GH nanoparticles *in situ*. The method developed in this study is simple, reproducible and environmentally benign. And the resulting GH nanoparticles exhibit high relaxivity and long intravascular half-life for MRI. Therefore, these novel hybrid nanoparticles will show promise in medical imaging.

2. Materials and methods

2.1. Materials

Chemicals. All chemicals were purchased from Sigma-Aldrich and used as-received. Ultrapure Millipore DI water (18.2 MΩ cm resistivity at 25 °C) was used. Animal procedures were in agreement with the guidelines of the Institutional Animal Care and Use Committee of Tongji University.

2.2. Synthesis of high relaxivity GH nanoparticles

In a typical experiment, aqueous gadolinium chloride solution (56.0 mg in 15.0 mL DI water) was added to BSA solution (15 mL, 50 mg mL⁻¹) slowly under vigorous stirring. NaOH solution (1.5 mL, 1.0 M) was introduced 3.0 min later, and the reaction was allowed to proceed under vigorous stirring at room temperature. After one hour, the solution was dialyzed against DI water to remove excess Gd³⁺. The prepared gadolinium-based hybrid nanoparticles were dialyzed against DI water to remove excess Gd³⁺ before freeze-drying. This step was used to enhance dissolution of the freeze-dried gadolinium-based hybrid nanoparticles in PBS buffer. The purified solution was then freeze-dried. The dried GH nanoparticles were dissolved in 3.0 mL PBS (10 mM, pH 7.4) for use. The concentration of Gd³⁺ was measured with ICP-AES. 50 µL of purified GH nanoparticles were diluted to 10.0 mL with nitrate solution, and the concentration nitrate solution was 3% w/v. The resulting solution was used for ICP-AES measurement.

2.3. Materials characterization

Aqueous GH nanoparticles were studied using a Tecnai G² F20 TEM operating at an acceleration voltage of 200 kV. The dispersion property of GH nanoparticles in solution was measured using a particle size analyzer (Nano ZS, Malvern). The elemental analysis was performed on an IRIS Intrepid (Thermo Elemental) ICP-AES system (the lowest detection limit of Gd³⁺ is 0.02 ppm). XPS experiments were carried out on a RBD upgraded PHI-5000C ESCA system (Perkin Elmer) with Mg Kα radiation ($h\nu = 1253.6$ eV) or Al Kα radiation ($h\nu = 1486.6$ eV). In general, the X-ray anode was run at 250 W and high voltage was kept at 14.0 kV with a detection angle at 54°. The pass energy was fixed at 23.5, 46.95 or 93.90 eV to ensure sufficient resolution and sensitivity. The base pressure of the analyzer chamber was 5×10^{-8} Pa. The sample was directly pressed to a self-supported disk (10 × 10 mm) and mounted on a sample holder then transferred into the analyzer chamber. The whole spectra (0–1100 (1200) eV) and the narrow spectra of all elements with much high resolution were recorded by using RBD 147 interface (RBD Enterprises, USA) with the AugerScan 3.21 software. Binding energies were calibrated by using the containment carbon (C1s = 284.6 eV). The data analysis was carried out by using the RBD AugerScan 3.21 software provided by RBD Enterprises or XPSPeak 4.1 by Raymund W.M. Kwok (The Chinese University of Hong Kong, China).

2.4. Colloidal and chemical stability test

The prepared GH nanoparticles (10 µL, 24.2 mM of Gd³⁺) were respectively incubated with serum (1.0 mL) at 37 °C for 24 hours and 4 °C for 25 days. Then, droplets from the incubated solution were visualized on TEM. The leakage of Gd³⁺ from the prepared GH nanoparticles was verified by ICP-AES. 200 µL of dissolved GH nanoparticles was ultrafiltrated with centrifuge filter tube (3 K, MWCO, PALL). The filtrate was collected for ICP-AES analysis.

This journal is © The Royal Society of Chemistry 2012

J. Mater. Chem., 2012, **22**, 14494–14501 | 14495

2.5. *In vitro* relaxometry

The longitudinal and transverse relaxation times were measured using a 1.41 T minispec mq 60 NMR Analyzer (Bruker, Germany) at 37 °C. The *in vitro* MR images were obtained using a MicroMR-25 mini MRI system (Niumag Corporation, Shanghai, China). The measurement conditions were as follows: T_1-weighted sequence: spin echo, TR/TE = 100.0/1.0 ms, matrix acquisition = 96 × 96, NS = 2, FOV = 22 mm × 22 mm, thickness = 5 mm, 0.535 T, 32.0 °C.

2.6. *In vivo* MR imaging

In vivo MR imaging was performed on a 1.5 T MR imaging system (GE Signa Excite) using an anesthetized mouse (mass *ca.* 20 g, *n* = 3 for the prepared GH nanoparticles of agent). Imaging was performed before, and at intervals after, intravenous injection (*via* the tail vein) of 0.05 mmol Gd per kg body weight of the agent. For illustrating the difference, one mouse was imaged after an intravenous injection of 0.1 mmol Gd per kg of Gd–DTPA. Images were obtained at baseline (prior to injection) and at subsequent intervals following injection, using a fat-saturated 3D gradient echo imaging sequence (TR/TE = 11.3/2.1 ms, four signal averages, 15° flip angle, 56 slices, 0.8 mm thick, acquisition time = 30 s). All image post-processing was performed using the Advantage Workstation 4.3 (AW4.3, General Electric Healthcare).

2.7. Cytotoxicity assay

The *in vitro* cytotoxicity was measured using 3-(4,5-dimethylth-iazol-2-yl)-2,5-diphenyltetrazolium bromide (MTT) assay. L929 cells growing in log phase were seeded into a 96-well cell-culture plate at 5 × 10³ per well and then incubated for 24 h at 37 °C under 5% CO$_2$. DMEM supplemented with 10% FBS (Fetal Bovine Serum) solutions of GH nanoparticles (100 μL per well, containing 1% HEPES) at concentrations of 0.48, 2.4, 12, 60, 300 μM (Gd^{3+}) were added to the wells of the treatment group, and DMEM containing 1% HEPES (100 μL per well) to the negative control group, respectively. The cells were incubated for 24 h, 48 h and 96 h at 37 °C under 5% CO$_2$. Subsequently, 10 μL MTT (5 mg mL^{-1}) was added to each well and incubated for an additional 4 h at 37 °C under 5% CO$_2$. After the addition of dimethylsulfoxide (DMSO, 150 μL per well), the assay plate was allowed to stand at room temperature for 10 minutes. A Tecan Infinite M200 monochromator-based multi-function microplate reader was used to measure the OD570 (*A* value) of each well with background subtraction at 690 nm. The following formula was used to calculate the viability of cell growth: cell viability (%) = (mean of *A* value of treatment group/mean of *A* value of control) × 100.

Cell apoptosis. Flow cytometry was used to analyze apoptosis of L929 cells after the treatment with GH nanoparticles. Seventy-two hours after treatment by GH nanoparticles, cells were trypsinized, stained with Annexin V-FITC and propidium iodide (PI) using the Annexin V-FITC Apoptosis Detection Kit I (BD Biosciences). The percentage of apoptotic cells was quantified by a BD LSRII flow cytometry (PI-positive indicated cell necrosis, while Annexin-V positive indicated cell apoptosis). Annexin V-FITC negative and PI positive indicates cell necrosis, while Annexin-V positive and PI negative indicates early apoptosis. Viable cells are both Annexin V-FITC and PI negative, and the cells in late apoptosis are both Annexin V-FITC and PI positive.

2.8. *In vivo* biodistribution and toxicity studies

Kunming mice (25 to 30 g of body weight) were purchased from the Second Military Medical University (Shanghai, China). Animal procedures were in agreement with the guidelines of the Institutional Animal Care and Use Committee of Tongji University. GH nanoparticles at a total dose of 0.05 mmol Gd per kg body weight were injected into Kunming mice (*n* = 3) *via* the tail vein.

In vivo biodistribution studies: major organs were removed from mice injected with GH nanoparticles 14 days post-injection after complete anesthesia. The removed organs were pulverized and treated with nitric acid. The organ nitric acid solutions were heated at 90 °C for two hours, and then filtered. The filtrates were ready for ICP analysis.

Histology studies: tissues were harvested from mice injected with GH nanoparticles 14 days post-injection. Mice were sacrificed after complete anesthesia. The liver and kidney were removed, and fixed in paraformaldehyde, embedded in paraffin, sectioned, and stained with hematoxylin and eosin. The histological sections were observed under an optical microscope.

3. Results and discussion

3.1. Synthesis and characterization of the GH nanoparticles

The synthetic scheme of GH nanoparticles is described in Fig. 1A. Briefly, aqueous gadolinium chloride solution is added to BSA solution slowly under vigorous stirring. NaOH solution is introduced subsequently, and the reaction is allowed to proceed under vigorous stirring at room temperature. After one hour, the solution is dialyzed against deionized water to remove excess Gd^{3+}. The resulting gadolinium-based hybrid nanoparticles *in situ* are round-like, consisting of Gd(OH)$_3$ and Gd$_2$O$_3$ as the core and BSA as the scaffold and coating material. The reaction that proceeded in absence of BSA produces only large insoluble aggregates, an indication that BSA is required for stabilizing GH nanoparticles.

Transmission electron microscopy (TEM) image (Fig. 1B) of the GH nanoparticles exhibit a round-like geometry with a uniform size, with an average size of 4.8 nm. This is consistent to
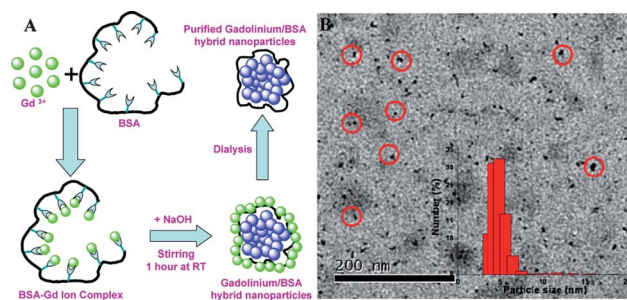

Fig. 1 Schematic of the bioinspired synthesis of GH nanoparticles. (A) The formation of GH nanoparticles in BSA/NaOH solution, and (B) TEM and DLS images (inset) of as-prepared GH nanoparticles.

the experimental results of the dynamic light scattering (DLS) as shown in the inset of Fig. 1B (also see Fig. S1 and S2† in ESI for enlarged photos). BSA is selected in the synthesis of GH nanoparticles for the following features. BSA is an important blood protein with high molecular weight and is composed of hundreds of amino acid residues. BSA contains abundant active chemical groups, such as carboxyl groups in aspartic and glutamate residues, thiol groups in cysteine, and eight disulfide bonds. These groups play a role in the formation of multiple metal complexes,[34] which is expected to favor the subsequent alkali-triggered agglomeration into templated GH nanoparticles. The BSA–Gd^{3+} mixture solution appears cloudy and opaque before the addition of NaOH. This indicates the interaction of BSA molecules with Gd^{3+}. After adding NaOH, the solution becomes optically transparent. The BSA protein then undergoes structural changes and transforms into its unfolded or tertiary configuration at alkaline environment. Such unfolded or denatured BSA is much efficient in controlling the crystal growth. In addition to the scaffolding and capping properties, BSA also holds abundant active chemical groups, which are favorable to post surface modifications with functional ligands.

The composition of the as-synthesized material was investigated by using X-ray photoelectron spectroscopy (XPS) analysis. The oxidation state of the GH nanoparticles was determined by XPS. The Gd 4d spectrum is deconvoluted into two components centered at binding energies of 141.2 and 143.5 eV, which are assigned to $Gd(OH)_3$ and Gd_2O_3, respectively (Fig. 2A). The O 1s spectrum shows three peaks (Fig. 2B), the peaks at 530.5 eV and 531.5 eV correspond to the oxygen in Gd_2O_3 and $Gd(OH)_3$ respectively. The peak at 532.6 eV originates from the oxygen in the carbonyl and carboxyl groups present in BSA protein. These results are in good agreement with the previously published XPS studies on gadolinium-based compounds.[27,35–38]

CAs used in body imaging require good colloidal stability. The easy-aggregated nanoparticle-based CAs must be evenly distributed with serum in vascular. The GH nanoparticles in this study are dispersed well in serum for 24 hours at 37 °C, and for 25 days at 4 °C in vitro (see Fig. S3† in ESI). The ICP-AES experimental results show that there is no Gd^{3+} leakage from the nanoparticles. Both TEM and ICP-AES analysis indicate that the GH nanoparticles are colloidal and chemically stable. The BSA-directed synthesis method has been previously used for the preparation of gold nano-cluster[29] and particles.[39] The GH nanoparticles synthesized in this study are particularly designed and developed with a unique structure consisting a gadolinium hydroxide/gadolinium oxide core and BSA coating, resulting in stable monodispersed particles in water.

3.2. In vitro relaxivity characterization of the GH nanoparticles

To determine the relaxivity value of the GH nanoparticles water solution, longitudinal (T_1) and transverse proton relaxation times (T_2) were measured as a function of gadolinium ion concentration at 1.41 T, 37 °C. The different concentrations of GH nanoparticles and Gd–DTPA for relaxivity characterization were obtained by dilution with deionized water. As shown in Fig. 3A, the GH nanoparticles exhibit high r_1 and r_2 values of 15.0 and 19.7 s^{-1} per mM of Gd^{3+}, respectively. The r_2/r_1 value of 1.3 indicates that the GH nanoparticle has a significant advantage as a positive CAs. The r_1 value of 15.0 is much higher among all reported gadolinium-based nanoparticle systems (see Table S1† in ESI). It shows a four-fold increase in the molar longitudinal relaxivity compared with that of Gd–DTPA ($r_1 = 3.7$ s^{-1} per mM of Gd^{3+}, shown in Fig. 3C). The transverse relaxivity is also significantly higher ($r_2 = 19.7$ s^{-1} per mM of Gd^{3+}) than that of Gd–DTPA in solution ($r_2 = 4.6$ s^{-1} per mM of Gd^{3+}). The relaxivity of the GH nanoparticles is about the same as the commercial Vasovist MRA CAs when bound with HSA (human Serum albumin). The relaxivity of unbound Vasovist is 6.6 s^{-1} per mM of Gd^{3+}, and increased to ~20 s^{-1} per mM of Gd^{3+} when bound with HSA. The high relaxivity of the GH nanoparticles is particularly useful in dose reduction, which is desirable for patients with weak kidney function.[40] For further comparison, T_1-weighted MR images of GH nanoparticles and Gd–DTPA with various concentrations of Gd^{3+} were obtained. As can be seen from Fig. 3B and D, the MR signal intensity of GH nanoparticles is much stronger than that of Gd–DTPA.

Fig. 3 The r_1 and r_2 relaxivity curves are obtained from solutions of GH nanoparticles (A) and commercial Gd–DTPA (C); T_1-weighted MR images of GH nanoparticles (B) with various concentrations (from 0.01 to 0.2 mM Gd^{3+}), and commercial Gd–DTPA (from 0.1 to 2.5 mM Gd^{3+}) (D). The samples are diluted with deionized water.
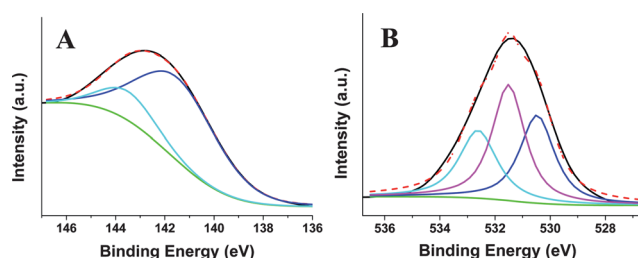

Fig. 2 Gd (4d) (A) and O (1s) (B) XPS spectrum of GH nanoparticles. The black lines are the experimentally measured data points; dash dot lines are the data-fitted; green lines are the background, and other peaks of different colours are corresponding to the Gd-components analysed by XPSPeak 4.1 software.
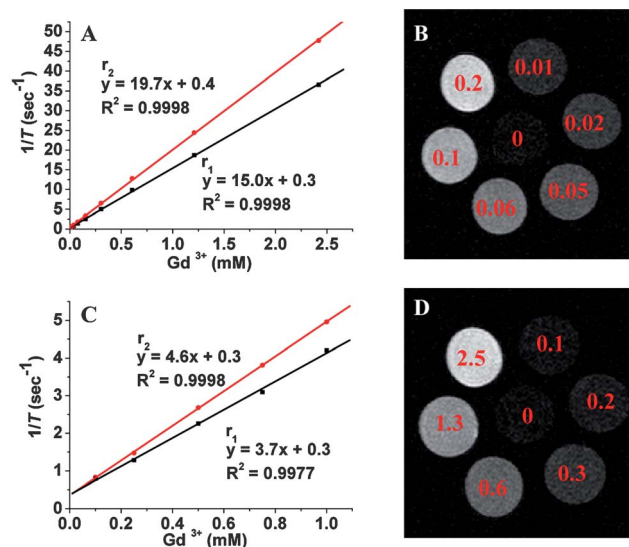
3.3. In vivo MRI measurement and biodistribution of GH nanoparticles

Fig. 4 shows maximum intensity projections (MIP) from the 3D images acquired *in vivo*. The first one was taken at baseline (left). The first image post injection of GH nanoparticles (5 min) shows good MR signal enhancement in the vessels, and this MRI enhancement is illustrated by a movie (see ESI†). The residual blood pool hyper-intensity in aortic 60 min post injection indicates the longevity of the agent in the blood pool with significant residual enhancement of the vasculature. One hour after injection, the aortic MR signal is greatly reduced and most of the GH nanoparticles are located in the liver, resulting in liver MR signal enhancement (Fig. 4A). The dynamic process of the MR signal transformation is further described in the ESI (see Fig. S4†). The *in vivo* MRI indicates that the GH nanoparticles can be used as both blood pool and liver CAs. The vascular half-life is over 60 min. Currently, there are few CAs that can be used for both blood pool and liver MRI. The commercially available superparamagnetic particles (SPIO) with predominant T_2 shortening effect have also been referred to as BPCAs, but they are disadvantaged by short vascular half-lives of less than 10 min due to endocytosis in the liver, spleen, and other reticuloendothelial system (RES) tissues. To illustrate the difference, the commercial Gd–DTPA with weak enhancement of the vasculature is cleared from the body within 100 min with hyper-intensity visible quickly in the bladder (Fig. 4B). Gadomer-17 is a new macromolecular gadolinium-based MRA CAs currently in clinical development. However, it is rapidly eliminated from the body, mainly *via* glomerular filtration.[41] Gadolinium-based small molecules with reversible protein binding have steady-state phase with a broad time window enabling high-resolution angiography. However, the liver imaging with these CAs needs further improvements.

No excretion to the bladder was observed for GH nanoparticles, which leaked to the extravascular space and eventually into the tissues, especially in the liver. This is due to the hydrodynamic diameter of the prepared GH nanoparticles being close to the glomerular filtration-size threshold.[42] Uptake of GH nanoparticles by the stomach is observed as early as 1 h post injection, and it is found in the large intestine 2 h later (Fig. S5†). The mouse injected with the GH nanoparticles was tracked by MRI at various time points (Fig. 5). The results show that the MR signal intensity in the liver reduces in a large degree at day 14, which demonstrates excretion of the GH nanoparticles from the body gradually. The metabolic behavior of GH nanoparticles is similar to that of the reported HA–(EDA–DTPA–Gd) blood pool CAs.[43] In order to evaluate the *in vivo* clearance process and biodistribution of the GH nanoparticles, mice were injected with 0.05 mmol Gd per kg body weight of GH nanoparticles through the tail vein. At different time points post-injection, mice were anesthetized, and sacrificed. The main organs were taken out for inductively coupled plasma atomic emission spectroscopy (ICP-AES) analysis of Gd^{3+} (Fig. 6). ICP analysis shows that GH nanoparticles uptake and retention took place primarily in the liver, spleen and large intestine with few GH nanoparticles accumulating in the heart, the kidney or the lung. The concentration of Gd^{3+} in the liver decreased gradually. And GH nanoparticles were found in the large intestine during the whole
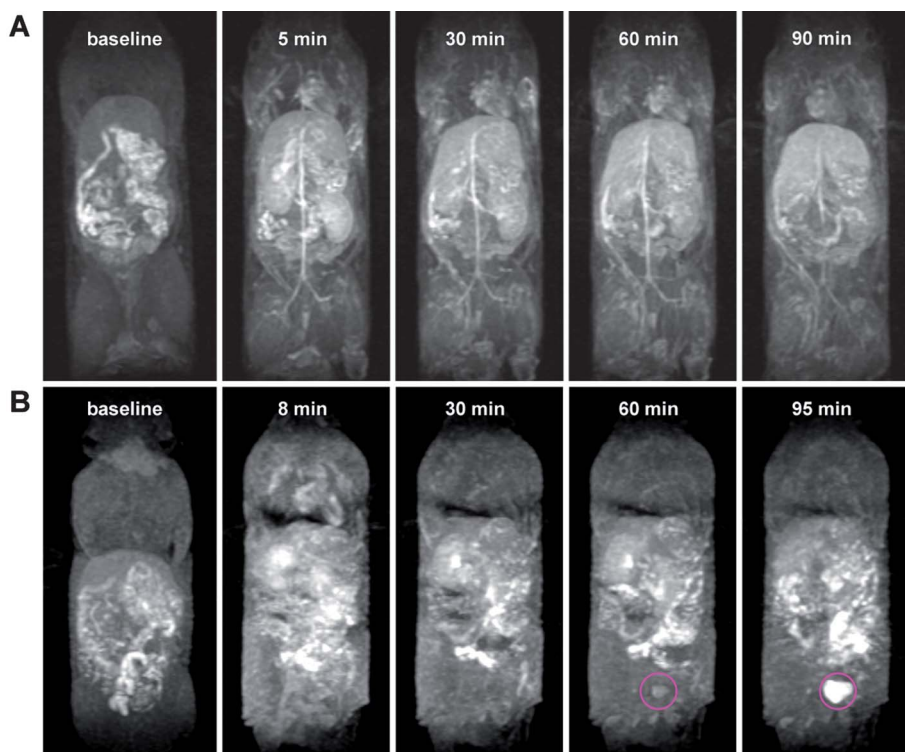

Fig. 4 Maximum intensity projections (MIP) from the 3D images acquired from the mouse intravenous-injected with GH nanoparticles (A) and commercial Gd–DTPA (B). Image is taken at baseline followed by the images at intervals after intravenous injection. The bladder of the mouse injected with commercial Gd–DTPA is indicated by a pink circle. The MRI enhancement is observed in the bladder at 60 min after injection.
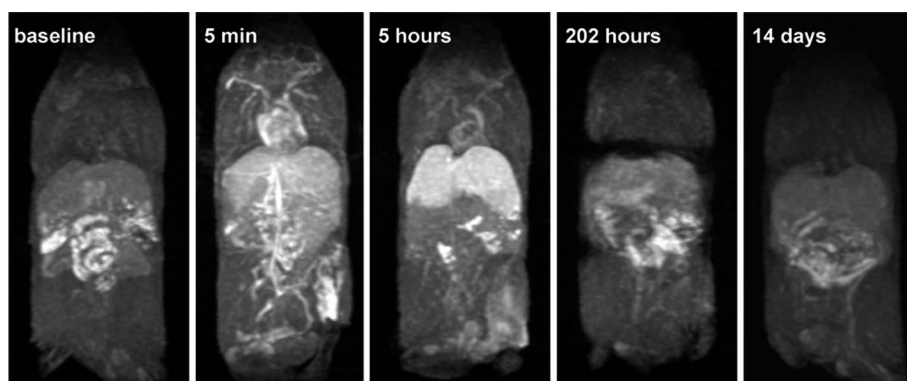
Fig. 5 MIPs from the 3D images acquired from GH nanoparticles, images were taken at baseline followed by the images at 5 minutes, 5 hours, 202 hours and 14 days after intravenous injection.
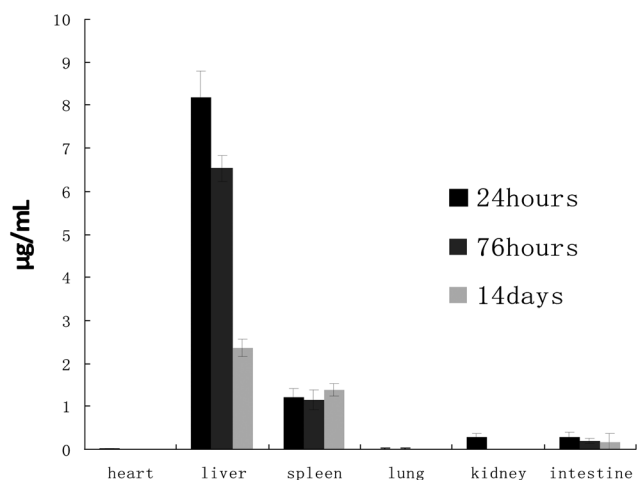

Fig. 6 Biodistribution of particles in organs of mice with intravenous injection of GH nanoparticles (0.05 mmol kg^{-1}) at different time points. Error bars were based on triplet measurements.

research period. These were consistent with that of *in vivo* MRI. The work on modification of GH nanoparticles for rational metabolism *in vivo* is in progress in our lab.

There are two primary routes of clearance of nanoparticles from the body. One is the renal filtration with excretion into urine; and the other is hepatobiliary (HB) processing with excretion into bile.[43] Clearance of nanoparticles is determined primarily by size and charge. Nanoparticle size, however, correlates most strongly with clearance dynamics, dominated by the particles below the glomerular filtration-size threshold, of non-specific adsorption to tissues, and those undergoing renal clearance. Those with sizes over this threshold are more easily trapped by the liver and RES system.[44] The clearance studies on silica nanoparticles with 20–25 nm suggest an initial uptake of the nanoparticles by the RES system, followed by their gradual degradation and excretion *via* the HB mechanism over a period of 15 days.[45] Liu *et al.* reported the near-complete clearance of single-walled carbon nanotubes (SWNTs) functionalized with polyethylene-glycol (PEG) from mice *via* the HB and renal pathways in approximately 2 months.[46] In this study, the clearance route of the GH nanoparticles are mainly *via* HB processing with excretion into bile due to those beyond the glomerular

filtration-size threshold. This has been investigated and verified by ICP analysis and MRI tracking.

3.4. Toxicity study of GH nanoparticles

Overall, no adverse reactions such as weight loss and death were observed in any mice that received GH nanoparticles three months after the *in vivo* experiments. The cytotoxicity test was conducted for GH nanoparticles on normal L929 cells. The 3-(4,5-dimethylthiazol-2-yl)-2,5-diphenyltetrazolium bromide (MTT) result indicates that the GH nanoparticles are biocompatible. The viabilities of L929 cells incubated with GH nanoparticles at various Gd concentrations, even at 300 μM of Gd^{3+} for 96 hours are over 90% (Fig. 7). Cell apoptosis results (Fig. 8) also indicate GH nanoparticles are biocompatible with cells.

To continue the investigation of toxicity, histological assessment of tissues was conducted to determine whether or not the GH nanoparticles cause tissue damage, inflammation, or lesions from toxic exposure. Analysis was performed on the tissues obtained from the harvested organs (liver and kidney) to assess signs of potential toxicity. Liver tissue was chosen for analysis, since GH nanoparticles are cleared from the liver, while the
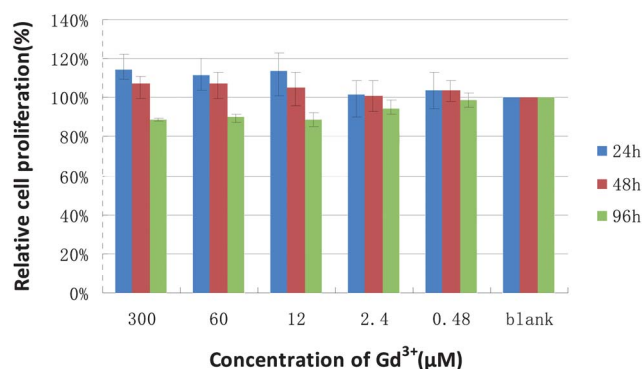

Fig. 7 The viability of L929 cells incubated with GH nanoparticles. GH nanoparticles are incubated with L929 cells at various Gd^{3+} concentrations for 24, 48 and 96 hours and viability is measured using 3-(4,5-dimethylthiazol-2-yl)-2,5-diphenyltetrazolium bromide (MTT) assay. Viability measurements are normalized to cells grown in the absence of any particles.
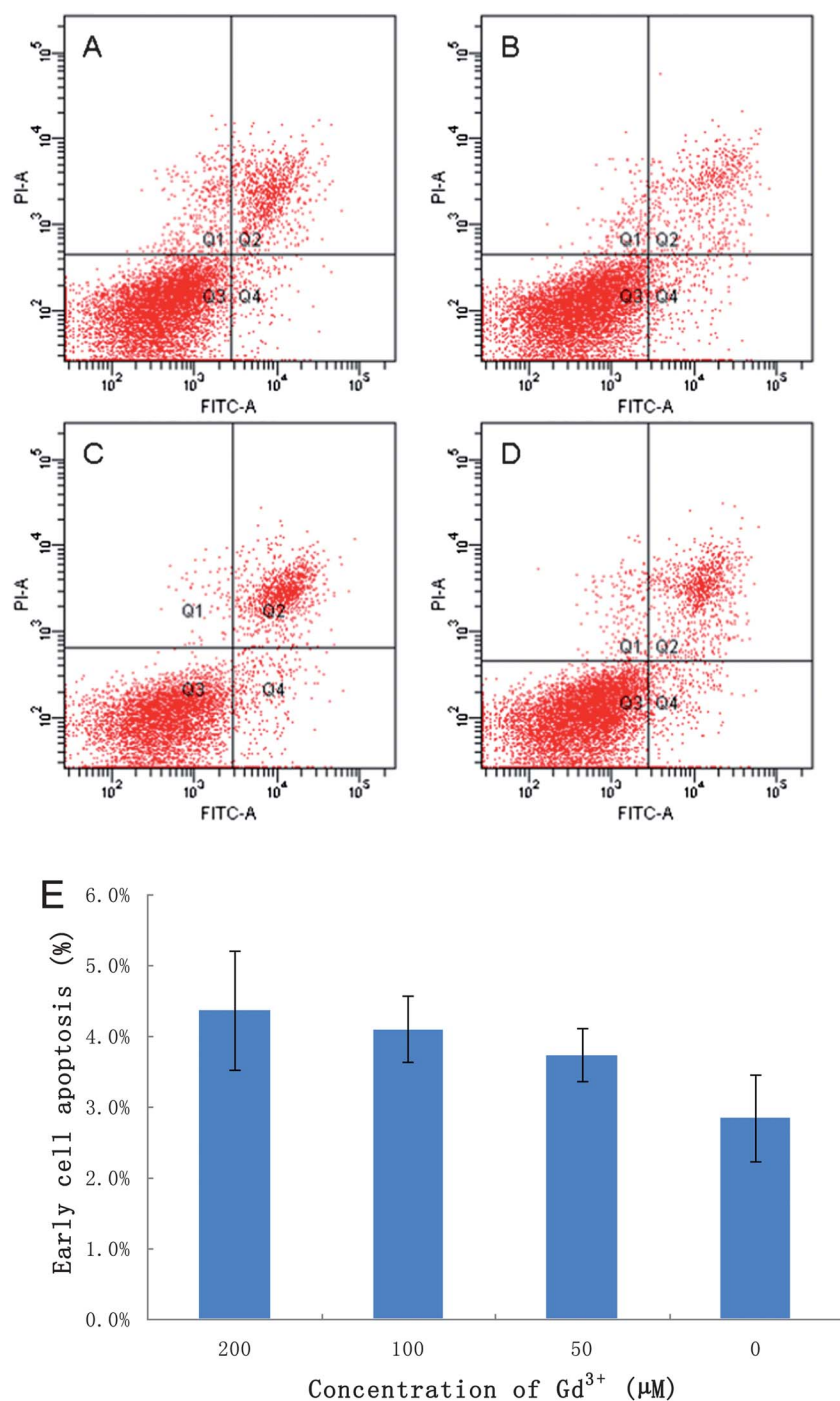
This journal is © The Royal Society of Chemistry 2012

J. Mater. Chem., 2012, **22**, 14494–14501 | 14499

Fig. 8 Flow cytometry analysis of cell apoptosis. L929 cells were cultured with 0 (A, the control), 50 (B), 100 (C) and 200 μM (Gd^{3+}) (D) of GH nanoparticles. Bar graph shows percentages of early cell apoptosis in response to a 72 hour incubation with different Gd ion concentrations (E). Seventy-two hours after the treatment, cells were trypsinized, stained with Annexin V-FITC and PI. PI positive indicates cell necrosis, while Annexin V positive indicates cell apoptosis. PI positive/Annexin V negative indicates cell necrosis, while Annexin V positive/PI negative and Annexin V positive/PI positive indicate early apoptosis and late apoptosis respectively.

kidney is tender to Gd exposure. As seen in Fig. 9, the structures of liver and kidney organs from the exposed mice were normal. Hepatocytes in the liver samples appeared normal, and there were no inflammatory infiltrates or liver fibrosis. The glomerulus structure could be distinguished easily in the kidney samples. No necrosis was found in both of the tissues.

Such a good biocompatibility is attributable to the green chemical synthesis and BSA biomolecular coating. High biocompatibility and long lifetime in the blood pool (in excess of 1 h) and liver indicate that the GH nanoparticles prepared in this study are ideal candidates for MRA and liver specific MRI application.
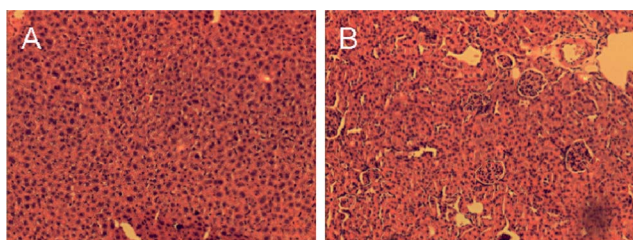
Fig. 9 Hematoxylin and eosin-stained tissue sections from mice injected with GH nanoparticles 14 days post-injection. Tissues were harvested from liver (A) and kidney (B).

4. Conclusions

In summary, we have developed a novel and simple method for the preparation of high relaxivity GH nanoparticles as positive blood pool and liver specific MRI CAs. The BSA-coated GH nanoparticles exhibit good biocompatibility and strong MRI enhancement both *in vitro* and *in vivo*. The *in vivo* MRI analysis indicates that these materials are ideal candidates for blood pool and liver MRI. Considering multiple advantages of the BSA-coated GH nanoparticles including simple synthesis, good biocompatibility and stability, and high relaxivity and long intravascular half-life, these novel hybrid nanoparticles will show promise in medical imaging.

References

1 T. Allkemper, W. Heindel, H. Kooijman, W. Ebert and B. Tombach, *Invest. Radiol.*, 2006, **41**, 97–104.
2 C. M. van Bemmel, O. Wink, B. Verdonck, M. A. Viergever and W. J. Niessen, *IEEE Trans. Med. Imaging*, 2003, **22**, 645–652.
3 C. Nolte-Ernsting, G. Adam, A. Bucker, S. Berges, A. Bjornerud and R. W. Gunther, *AJR, Am. J. Roentgenol.*, 1998, **171**, 107–113.
4 E. Unger, D. Cardenas, A. Zerella, L. L. Fajardo and C. Tilcock, *Invest. Radiol.*, 1990, **25**, 638–644.
5 M. Ogawa, C. A. Regino, B. Marcelino, M. Williams, N. Kosaka, L. H. Bryant, Jr, P. L. Choyke and H. Kobayashi, *Bioconjugate Chem.*, 2010, **21**, 955–960.
6 M. Goyen, *Vasc. Health Risk Manage.*, 2008, **4**, 1–9.
7 P. Perreault, M. A. Edelman, R. A. Baum, E. K. Yucel, R. M. Weisskoff, K. Shamsi and E. R. Mohler, 3rd, *Radiology*, 2003, **229**, 811–820.
8 J. H. Feng, X. J. Li, F. K. Pei, G. Y. Sun, X. Zhang and M. L. Liu, *Magn. Reson. Imaging*, 2002, **20**, 407–412.
9 M. Essig, M. Rohrer, F. Giesel, J. Tuttenberg, M. A. Weber, H. Michaely, L. Gerigk and M. Voth, *Eur. Radiol.*, 2010, **20**, 218–226.
10 R. B. Lauffer and T. J. Brady, *Magn. Reson. Imaging*, 1985, **3**, 11–16.
11 A. D. Sherry, W. P. Cacheris and K. T. Kuan, *Magn. Reson. Med.*, 1988, **8**, 180–190.
12 J. M. Wild, J. Woodrow, E. J. van Beek, B. Misselwitz and R. Johnson, *Contrast Media Mol. Imaging*, 2010, **5**, 39–43.
13 C. Corot, P. Robert, J. M. Idee and M. Port, *Adv. Drug Delivery Rev.*, 2006, **58**, 1471–1504.
14 C. Platas-Iglesias, L. Vander Elst, W. Z. Zhou, R. N. Muller, C. F. G. C. Geraldes, T. Maschmeyer and J. A. Peters, *Chem.–Eur. J.*, 2002, **8**, 5121–5131.
15 J. L. Bridot, A. C. Faure, S. Laurent, C. Riviere, C. Billotey, B. Hiba, M. Janier, V. Josserand, J. L. Coll, L. Vander Elst, R. Muller, S. Roux, P. Perriat and O. Tillement, *J. Am. Chem. Soc.*, 2007, **129**, 5076–5084.
16 H. Hifumi, S. Yamaoka, A. Tanimoto, D. Citterio and K. Suzuki, *J. Am. Chem. Soc.*, 2006, **128**, 15090–15091.
17 S. Kommareddy and M. Amiji, *J. Pharm. Sci.*, 2007, **96**, 397–407.
18 W. J. Rieter, K. M. L. Taylor, H. Y. An, W. L. Lin and W. B. Lin, *J. Am. Chem. Soc.*, 2006, **128**, 9024–9025.
19 S. Srivastava, R. Awasthi, N. S. Gajbhiye, V. Agarwal, A. Singh, A. Yadav and R. K. Gupta, *J. Colloid Interface Sci.*, 2011, **359**, 104–111.
20 M. Bottrill, L. K. Nicholas and N. J. Long, *Chem. Soc. Rev.*, 2006, **35**, 557–571.
21 A. Yurt and N. Kazanci, *J. Mol. Struct.*, 2008, **892**, 392–397.
22 P. Caravan, J. J. Ellison, T. J. McMurry and R. B. Lauffer, *Chem. Rev.*, 1999, **99**, 2293–2352.
23 K. Luo, G. Liu, B. He, Y. Wu, Q. Y. Gong, B. Song, H. Ai and Z. W. Gu, *Biomaterials*, 2011, **32**, 2575–2585.
24 E. D. Brown and R. C. Semelka, *Top. Magn. Reson. Imag.*, 1995, **7**, 82–89.
25 T. Bui, J. Stevenson, J. Hoekman, S. R. Zhang, K. Maravilla and R. J. Y. Ho, *PLoS One*, 2010, **5**, e13082.
26 K. Hekimoglu, Y. Ustundag, A. Dusak, B. Kalaycioglu, H. Besir, H. Engin and O. Erdem, *Eur. J. Radiol.*, 2011, **77**, 468–472.
27 A. T. M. A. Rahman, K. Vasilev and P. Majewski, *J. Colloid Interface Sci.*, 2011, **354**, 592–596.
28 K. M. Towe and H. A. Lowenstam, *J. Ultrastruct. Res.*, 1967, **17**, 1–13.
29 J. Xie, Y. Zheng and J. Y. Ying, *J. Am. Chem. Soc.*, 2009, **131**, 888–889.
30 N. Nuraje, S. Mohammed, L. Yang and H. Matsui, *Angew. Chem., Int. Ed.*, 2009, **48**, 2546–2548.
31 N. Ma, A. F. Marshall and J. Rao, *J. Am. Chem. Soc.*, 2010, **132**, 6884–6885.
32 H. Liang, T. E. Angelini, J. Ho, P. V. Braun and G. C. Wong, *J. Am. Chem. Soc.*, 2003, **125**, 11786–11787.
33 I. A. Banerjee, L. Yu and H. Matsui, *J. Am. Chem. Soc.*, 2005, **127**, 16002–16003.
34 M. M. Yamashita, L. Wesson, G. Eisenman and D. Eisenberg, *Proc. Natl. Acad. Sci. U. S. A.*, 1990, **87**, 5648–5652.
35 D. F. Mullica, C. K. C. Lok, H. O. Perkins, G. A. Benesh and V. Young, *J. Electron Spectrosc. Relat. Phenom.*, 1995, **71**, 1–20.
36 F. Soderlind, H. Pedersen, R. M. Petoral, P. O. Kall and K. Uvdal, *J. Colloid Interface Sci.*, 2005, **288**, 140–148.
37 J. P. Zhou, C. L. Chai, S. Y. Yang, Z. K. Liu, S. L. Song, Y. L. Li and N. F. Chen, *J. Cryst. Growth*, 2004, **270**, 21–29.
38 J. Szade, J. Lachnitt and M. Neumann, *Phys. Rev. B: Condens. Matter Mater. Phys.*, 1997, **55**, 1430–1434.
39 Q. S. Wang, F. Y. Ye, T. T. Fang, W. H. Niu, P. Liu, X. M. Min and X. Li, *J. Colloid Interface Sci.*, 2011, **355**, 9–14.
40 F. Secchi, G. Di Leo, G. D. E. Papini, F. Giacomazzi, M. Di Donato and F. Sardanelli, *Eur. J. Radiol.*, 2011, **80**, 96–102.
41 B. Misselwitz, H. Schmitt-Willich, W. Ebert, T. Frenzel and H. J. Weinmann, *Magn. Reson. Mater. Phys., Biol. Med.*, 2001, **12**, 128–134.
42 M. Longmire, P. L. Choyke and H. Kobayashi, *Nanomedicine*, 2008, **3**, 703–717.
43 W. L. Zhu and D. Artemov, *Contrast Media Mol. Imaging*, 2011, **6**, 61–68.
44 J. S. Souris, C. H. Lee, S. H. Cheng, C. T. Chen, C. S. Yang, J. A. A. Ho, C. Y. Mou and L. W. Lo, *Biomaterials*, 2010, **31**, 5564–5574.
45 R. Kumar, I. Roy, T. Y. Ohulchanskky, L. A. Vathy, E. J. Bergey, M. Sajjad and P. N. Prasad, *ACS Nano*, 2010, **4**, 699–708.
46 Z. Liu, C. Davis, W. B. Cai, L. He, X. Y. Chen and H. J. Dai, *Proc. Natl. Acad. Sci. U. S. A.*, 2008, **105**, 1410–1415.

This journal is © The Royal Society of Chemistry 2012

J. Mater. Chem., 2012, **22**, 14494–14501 | 14501